EFFECT OF TURBULENCE MODELS ON CRITICALITY CONDITIONS IN SWIRLING FLOWS

Robert E. Spall
Department of Mechanical Engineering
University of South Alabama
Mobile, Alabama

and

Thomas B. Gatski
Theoretical Flow Physics Branch
NASA Langley Research Center
Hampton, Virginia

SUMMARY

The critical state of vortex cores downstream of vortex breakdown has been studied. Base vortical flows were computed using the Reynolds-averaged, axisymmetric Navier-Stokes equations. Standard $K-\varepsilon$, RNG and second-order Reynolds stress models were employed. Results indicate that the return to supercriticality is highly dependent on the turbulence model. The $K-\varepsilon$ model predicted a rapid return of the vortex to supercritical conditions, the location of which showed little sensitivity to changes in the swirl ratio. The Reynolds stress model predicted that the vortex remains subcritical to the end of the domain for each of the swirl ratios employed, and provided results in qualitative agreement with experimental work. The RNG model produced intermediate results, with a downstream movement in the critical location with increasing swirl. Calculations for which area reductions were introduced at the exit in a subcritical flow were also performed using the Reynolds stress model. The structure of the resulting recirculation zone was altered significantly. However, when area reductions were employed within supercritical flows as predicted using the two-equation models, no significant influence on the recirculation zone was noted.

INTRODUCTION

Over the past 30 years, considerable effort has been expended toward an understanding of the mechanisms inherent in the development and evolution of longitudinal vortices. This has been motivated, in part, by the desire to control and/or disable these vortices in applications such as the aircraft-wake-vortex hazard and submarine non-acoustic stealth. Perhaps in no application are the properties of swirling flows exploited to a greater extent than in the operation of gas turbine and industrial furnace combustion chambers. Here, a region of high swirl is induced at an entrance to the combustor liner, typically through a set of swirler vanes, resulting in a region of recirculating flow. This region acts as a fluid dynamic flameholder, providing a region of low velocity within which combustion may be sustained, and recirculating hot, unburned gases to the base of the flame.

This recirculating region is known as a vortex breakdown. Although several theories have been put forth to explain the breakdown phenomena, perhaps none are more widely recognized than the early works of Squire [1] and Benjamin [2]. By choosing certain functional forms for the base vortex flow, Squire reduced the nonlinear equations of motion (inviscid, steady) to a linear disturbance equation. He subsequently solved the equation to determine conditions under which a steady perturbation to the flow could exist. This condition, in terms of a swirl ratio, was taken as a limiting condition for which breakdown could occur. Benjamin examined this phenomena from a different perspective. He considered vortex breakdown to be a finite transition between two dynamically conjugate states of flow, similar to the occurrence of a hydraulic jump in open channel flow. The two states were a *subcritical* state, which was defined as a flow which could support standing waves, and a *supercritical* state, unable to support standing waves. In this context, the work of Squire defined a critical condition marking the interface between the two states.

The criticality condition has not received much attention from those computing numerical solutions to swirling flows, and flows containing vortex breakdown in particular. Of special interest is the region downstream of the breakdown. Immediately downstream, the flow is most assuredly subcritical (c.f. Tsai and Widnall [3]). However, as the axial velocity recovers and the swirl velocity decays, the flow may return to a supercritical state at some downstream location. The consequences of the failure of a swirling flow to return to supercriticality has been discussed by Escudier and Keller [4]. In that experimental study, it was shown that the upstream influence of an exit contraction on vortex breakdown was substantially greater when the flow remained subcritical compared to a flow that reverted to supercritical (upstream of the contraction). Escudier and Keller suggest that this phenomena might have significant consequences in the imposition of accurate outflow boundary conditions.

Most swirling flows of practical interest, such as the flow within a combustor, are turbulent. For numerical calculations of turbulent swirling flows, the choice of turbulence model is of vital importance. It is well known that the standard $K-\varepsilon$ model does a poor job of predicting strongly swirling flows (c.f. Jones and Pascau [5]). One of the consequences of choosing the $K-\varepsilon$ model is that the wake region near the vortex centerline (downstream of breakdown) recovers much more rapidly than has been shown to occur in experiments. On the other hand, second-order closure models contain the physics necessary to model strongly swirling flows, and tend to do a better job of predicting the recovery of the axial velocity component (c.f. Jones and Pascau [5]).

These varying predictive capabilities have consequences in terms of the criticality of the flow. That is, one would expect the $K-\varepsilon$ model to predict a return to criticality upstream of the position predicted by second-order Reynolds stress models. This behavior has been investigated to some extent by Hogg and Leschziner [6]. However, in that work swirl ratios were such that no recirculation zone was formed when the Reynolds stress model was employed. In addition, no direct calculations of the critical condition of the flow were made. However, the critical state (based on an inviscid analysis, c.f. Hall [7]) is not difficult to compute and thus the purpose of this research is to further investigate the criticality conditions of swirling flows downstream of turbulent vortex breakdown as predicted using several different turbulence models ($K-\varepsilon$, RNG (c.f. Yakhot et al. [8]) and differential Reynolds stress). Geometries both with and without an exit restriction are employed. The relationship and consequences (if any) of the state of the flow (in terms of criticality) to the outflow restriction and turbulence model employed will be determined.

NUMERICAL PROCEDURE

The incompressible, axisymmetric Reynolds-averaged Navier-Stokes equations are solved for the swirling flow within a combustor-type geometry. Although the governing equations are solved in general curvilinear coordinates, for purposes of brevity they are presented below in cartesian tensor form. The continuity and momentum equations are given as:

$$\frac{\partial u_i}{\partial x_i} = 0 \tag{1}$$

$$\frac{\partial u_i}{\partial t} + u_j \frac{\partial u_i}{\partial x_j} = -\frac{1}{\rho}\frac{\partial p}{\partial x_i} + \frac{\mu}{\rho}\nabla^2 u_i - \frac{\partial \tau_{ij}}{\partial x_j} \tag{2}$$

respectively, where u_i is the mean velocity, ρ is the density, μ is the viscosity, p is the mean pressure and $\tau_{ij} = \overline{u'_i u'_j}$ are the Reynolds stresses.

Turbulence Models

Although the turbulence models utilized in the present study are well documented in the literature, the equations are included for completeness. When the $K-\varepsilon$ or RNG models are employed, the Boussinesq hypothesis provides an expression for the Reynolds stresses is terms of the gradients of the mean flow as:

$$-\tau_{ij} = -\frac{2}{3}\delta_{ij}K + 2\nu_t S_{ij} \tag{3}$$

where ν_t is the turbulent viscosity, K is the turbulent kinetic energy and S_{ij} is the strain rate. The turbulent viscosity is expressed in terms of K and the dissipation rate ε as:

$$\nu_t = C_\mu \frac{K^2}{\varepsilon} \tag{4}$$

Transport equations for K and ε, respectively, are written as:

$$\frac{DK}{Dt} = \frac{\partial}{\partial x_i}\left(\frac{\nu_t}{\sigma_k}\frac{\partial K}{\partial x_i}\right) + 2\nu_t S_{ij}^2 - \varepsilon \tag{5}$$

$$\frac{D\varepsilon}{Dt} = \frac{\partial}{\partial x_i}\left(\frac{\nu_t}{\sigma_\varepsilon}\frac{\partial \varepsilon}{\partial x_i}\right) + 2\nu_t C_{\varepsilon 1}\frac{\varepsilon}{K}S_{ij}^2 - C_{\varepsilon 2}\frac{\varepsilon^2}{K} - \bar{R} \tag{6}$$

In the case of the standard $K-\varepsilon$ equation $\bar{R} = 0$. For the RNG model (see Yakhot et al. [8]):

$$\bar{R} = \frac{C_\mu \eta^3 (1 - \eta/\eta_0)}{1 + \beta\eta^3}\frac{\varepsilon^2}{K} \tag{7}$$

where $\eta = SK/\varepsilon$ and $S = (2S_{ij}S_{ij})^{1/2}$.

It remains to specify the constants in the above equations. For the $K-\varepsilon$ model the standard values for boundary layer flows ($C_\mu = 0.09$, $C_{\varepsilon_1} = 1.44$, $C_{\varepsilon_2} = 1.92$, $\sigma_k = 1.0$ and

$\sigma_\varepsilon = 1.3$) have been taken. For the RNG model, theoretical analysis yields that $C_{\varepsilon 2} = 1.68$, $C_{\varepsilon 1} = 1.42$, $\sigma_k = \sigma_\varepsilon = 0.72$, $\eta_0 = 4.38$ and $\beta = 0.012$.

The Reynolds stress model involves the solution of transport equations for the individual Reynolds stresses $\overline{u'_i u'_j}$. The following equations, employing the closure assumptions of Gibson and Launder [9], and Launder [10], are solved:

$$\frac{D\overline{u'_i u'_j}}{Dt} = \frac{\partial}{\partial x_k}\left(\frac{\nu_t}{\sigma_k}\frac{\partial}{\partial x_k}\overline{u'_i u'_j}\right) + P_{ij} + \Phi_{ij} - \varepsilon_{ij} \tag{8}$$

The production term is computed as:

$$P_{ij} = -\overline{u'_i u'_k}\frac{\partial u_j}{\partial x_k} + \overline{u'_j u'_k}\frac{\partial u_i}{\partial x_k} \tag{9}$$

The pressure/strain and dissipation terms are modeled as:

$$\Phi_{ij} = -C_3\frac{\varepsilon}{K}\left(\overline{u'_i u'_j} - \frac{2}{3}\delta_{ij}K\right) - C_4\left(P_{ij} - \frac{2}{3}\delta_{ij}P\right) \tag{10}$$

$$\varepsilon_{ij} = \frac{2}{3}\delta_{ij}\varepsilon \tag{11}$$

with values $C_3 = 1.8$ and $C_4 = 0.06$ assigned to the constants.

For each model wall functions based upon the assumption of a fully developed equilibrium turbulent boundary layer are utilized in the near wall region. This approach is deemed suitable since the physics of the problem are not dominated by near wall phenomena.

Solution Procedure

The above equations were solved using the commercial code FLUENT [11]. FLUENT utilizes a pressure-based control volume technique. Second-order upwind interpolation is used to provide values of variables on cell faces. Pressure-velocity coupling is implemented using the SIMPLEC algorithm [12]. Convergence of the solution is assumed when the sum of the normalized residuals for the conservation equations is decreased to a minimum of 1.0×10^{-3}. (The residual for a given equation consists of the summation of the unbalance in the equation for each cell in the domain.) Comparisons revealed that solutions converged by an additional factor of two were virtually indistinguishable. Since the above techniques are well known and widely discussed in the literature, they will not be elaborated upon here.

Geometry and Boundary Conditions

The geometric configuration is that of a prototypical combustor. The geometry near the expansion/breakdown region is shown with the computational grid superimposed in Figure 1. The domain was discretized using 170 (axial) and 40 (radial) grid points. Grid points were clustered near the breakdown region. The length of the domain is $40h$, where h is the radius at inflow. The expansion of area ratio 4:1 takes place over a length of $3h$. Note that the i=constant lines in the

physical grid occur at constant x — this is to facilitate calculation of the flow criticality. Additional calculations were made utilizing a 114 x 27 grid. No significant changes in the solutions were noted.

At inflow, a solid body rotation of the form $w = \Omega r$ has been specified (where w represents the circumferential velocity). The value of Ω was assigned values ranging form 0.75 to 1.5. The axial velocity has been taken as uniform, that is $u = 1.0$, and the turbulence intensity was set at 10%. At the outflow boundary, zero streamwise gradient conditions were enforced. The appropriateness of these conditions is confirmed by examining the distribution of the velocity contours (as shown in the Results section) near the outflow boundary. In addition, for each calculation the Reynolds number, based on the axial velocity and duct radius at inflow, was 100,000.

Criticality Calculations

Determination of the criticality of the flow is based the solution of the following ordinary differential equation (c.f. Benjamin [2] or Hall [7]):

$$\frac{\partial^2 F_c}{\partial r^2} - \frac{1}{r}\frac{\partial F_c}{\partial r} + \left[-\frac{1}{u}\frac{\partial^2 u}{\partial r^2} + \frac{1}{ru}\frac{\partial u}{\partial r} + \frac{1}{r^3 u^2}\frac{\partial \kappa^2}{\partial r} \right] F_c = 0 \qquad (12)$$

where $\kappa = rw$ is the circulation and F_c is a quasi-cylindrical perturbation shape function. Assumptions inherent in the above equation are that the fluid is inviscid, and that the flow is steady and axisymmetric. Thus, the criticality condition, as defined by Benjamin or Hall, is concerned only with the propagation or existence of axisymmetric waves on inviscid cores. However, we shall utilize the theory to predict the ability of high Reynolds number turbulent cores to support axisymmetric waves.

The radial distributions for u and $\bar{K}$ are available at any axial location from the mean flow calculations. The above equation is solved subject to the boundary conditions $F_c = 0$ and $\frac{\partial F_c}{\partial r}$ = constant at $r = 0$. The flow is subcritical if the solution curve passes through zero in the interval $0 < r < 2h$, supercritical if the solution does not pass through zero, and critical if the solution is zero at both $r = 0$ and $r = 2h$ (where $2h$ is the duct radius). The above equation is solved utilizing a second-order accurate modified Euler technique.

RESULTS

The behavior of each of the turbulence models in predicting the location of the return to criticality of the vortex is presented first. Following this, contours of constant axial velocity are examined, and the effects of outlet restrictions on the flow are discussed.

Mean flow calculations were performed for Ω=0.75, 1.125 and 1.5, utilizing the $K-\varepsilon$, RNG and Reynolds stress turbulence models. The axial location at which the vortex returned to a supercritical state was computed by solving an ordinary differential equation, as described earlier. In each case, the vortex was supercritical upstream and subcritical immediately downstream of the breakdown location. The results for return to supercriticality are summarized in Figure 2. The $K-\varepsilon$ model predicted a return to supercritical conditions at locations considerably upstream of that predicted by the other models. In addition, and contrary to what one would expect, the $K-\varepsilon$ model predicted that the location at which the vortex returned to a supercritical state was not

affected by changes in the swirl level at inflow. Conversely, the RNG model showed an expected sensitivity to increases in swirl. That is, as the swirl level at inflow was increased, the critical location moved downstream. In the case of the Reynolds stress model, the vortex remained subcritical to the exit for all swirl levels. We note that $\Omega = 0.75$ represented the approximate minimum swirl level for which a recirculation zone was formed using the Reynolds stress model. Consequently, calculations of vortex breakdown flows using Reynolds stress models will likely involve outflow boundary conditions imposed on subcritical flows (due to practical limitations on the length of the computational domain). However, this need not be the case for the two-equation models.

Escudier and Keller [4] have shown that the shape and internal structure of the recirculation region is strongly influenced by outlet restrictions if the restriction is imposed within a subcritical flow. To examine whether or not these effects are observed in numerical calculations, results have been computed using the Reynolds stress model for area reductions of 19% and 36% with $\Omega = 1.5$. The reductions extended over $33.67h \le x \le 40h$. Results are presented in terms of axial velocity contours in Figures 3a-c for the unrestricted case, the 19% reduction, and the 36% reduction, respectively. (For purposes of clarity, the contour plots have been scaled by a factor of 3 in the radial direction. In addition, the inner-most contour levels within the bubble structure represent the level $u = -0.1$.) It is clear that the 36% area reduction has a large effect on the shape of the aft portion of the bubble near the vortex centerline. The zero axial velocity contour undercuts this portion of the bubble, in effect lifting the recirculation zone off the axis. Note however, that the forward portion of the bubble remains virtually unaffected. In addition, a strong jet-like vortex core exists downstream of the breakdown. These features are in very good agreement with those observed by Escudier and Keller [4] in their experimental work. For the 19% area reduction case, the primary effects concern the rate of recovery of the axial velocity downstream of the breakdown. The shape and internal structure of the bubble remains similar to that of the unrestricted case. This result is also consistent with the results of Escudier and Keller. We do note that the geometry of Escudier and Keller was somewhat different than that employed in this study. In their study, a solid inner cylinder was included at the inflow plane, and a step expansion rather than a gradual expansion was used. Numerical convergence problems prevented our use of that geometry. However, the structure of the recirculation region for confined flows undergoing vortex breakdown does not appear to be overly sensitive to the inlet geometry.

It is of interest that the downstream measurements by Escudier and Keller were $0.39L$ upstream of the area reduction (where L was the distance between the inlet and the reduction). Thus, it is quite possible that for their cases in which the area reductions were very large, the flow actually returned to a supercritical state upstream of the restriction (but downstream of their last data point). That is, due to continuity the mean axial flow velocity increases with the square of the area reduction; however conservation of angular momentum dictates that the swirl velocity increase in a linear manner. Thus, the ratio of swirl to axial velocity generally decreases, resulting in a possible return to supercritical conditions. In fact, the authors found that for the low swirl case ($\Omega = 0.75$) area reductions on the order of 20% did result in the flow returning to a supercritical state slightly upstream of the area reduction. However, for the high swirl cases shown in Figures 3b-c, the vortex remained in a subcritical state to the exit.

Contours of constant axial velocity for the $K-\varepsilon$ and RNG models (without exit restrictions) are shown in Figures 4a-b, respectively for the case $\Omega = 1.5$. The differences in the axial

velocity distributions downstream of the breakdown region as predicted by these models and the Reynolds stress model are quite large. The rapid increases in the axial velocity for the $K-\varepsilon$ and RNG models (accompanied by equally rapid decreases in the swirl velocity) account for the rapid return to supercriticality. In addition, the internal structures of the bubbles predicted by these two-equation models differ considerably amongst themselves, and with that produced by the Reynolds stress model. Calculations were also made for the $K-\varepsilon$ and RNG models 36% area reductions. For the sake of brevity, we show only the results from the RNG model in Figure 4c. (Recall that for the two-equation models the vortex was supercritical upstream of the restriction.) As the figure reveals, virtually no difference in the axial extent or shape of the recirculation region resulted (when compared with the case in which no restriction was employed). This further confirms the experimental results of Escudier and Keller, and highlights the extreme sensitivity of strongly swirling flows to the turbulence model employed.

CONCLUSIONS

It is clear from the results of this study that wide differences exist in the predictions of two-equation and Reynolds stress turbulence models for return to supercriticality of swirling flows downstream of vortex breakdown. The results of the Reynolds stress model are in better agreement with experimental results for swirling flows (in similar geometries) as described by Escudier and Keller [4] than results predicted using two-equation models. Thus, the study further highlights the inappropriateness of using two-equation models to predict strongly swirling flows. The suggestion by Escudier and Keller that outflow restrictions might have a drastic effect on the structure of the breakdown as predicted through numerical solutions to the equations of motion was confirmed. Results revealed that for relatively large area reductions (on the order of 36%), the structure of the recirculation region may be greatly affected. However, for lesser reductions, the shape of the recirculation zone may be very similar to that resulting from the unrestricted geometry. Consequently, it does not appear that the requirements for the specification of outflow boundary conditions need be significantly more stringent for subcritical swirling flows than for supercritical flows, or for flows without swirl. This is fortunate—the persistent nature of the subcritical flow as revealed by the experiments of Escudier and Keller [4], and as predicted by the Reynolds stress model would severely restrict the predictive capability of many engineering-type calculations.

The authors plan future work in the area of combusting flows. For these calculations, accelerations in the axial velocity due to decreases in density should considerably alter the critical state of the flow.

REFERENCES

1. Squire, H.B. "Analysis of the Vortex Breakdown Phenomenon. Part I.," Aero Dept. Imperial Coll. London, Rep. 102, 1960.

2. Benjamin, T.B., "Theory of the Vortex Breakdown Phenomena," Journal of Fluid Mechanics, Vol. 14, 1962, pp. 593-629.

3. Tsai, C-Y. and Widnall, S.E., "Examination of Group-Velocity Criterion for Breakdown of Vortex Flow in a Diverging Duct," Physics of Fluids, Vol. 23, 1980, pp. 864-870.

4. Escudier, M.P. and Keller, J.J., "Recirculation in Swirling Flow: A Manifestation of Vortex

Breakdown," AIAA Journal, Vol. 23, January 1985, pp. 111-116.

5. Jones, W.P. and Pascau, A., "Calculation of Confined Swirling Flows with a Second Moment Closure," ASME Journal of Fluids Engineering, Vol. 111, September 1989, pp. 248-255.

6. Hogg, S. and Leschziner, M.A., "Computation of Highly Swirling Confined Flow with a Reynolds Stress Turbulence Model," AIAA Journal, Vol. 27, January 1989, pp. 57-63.

7. Hall, M.G., "Vortex Breakdown," Annual Review of Fluid Mechanics, Vol. 4, 1972, pp. 195-218.

8. Yakhot, V., Orszag, S.A., Thangam, S., Gatski, T.B. and Speziale, C.G., "Development of Turbulence Models for Shear Flows by a Double Expansion Technique," Physics of Fluids A, Vol. 4, No. 7, 1992, pp. 1510-1520.

9. Gibson, M.M. and Launder, B.E., "Ground Effects on Pressure Fluctuations in the Atmospheric Boundary Layer," Journal of Fluid Mechanics, Vol. 86, 1978, pp. 491-511.

10. Launder, B.E. "Second-Moment Closure: Present... and Future?," International Journal of Heat and Fluid Flow, Vol. 10, No. 4, 1989, pp. 282-300.

11. Fluent, Inc., Lebanon, NH, Fluent Users Guide.

12. Patankar, S.V. Numerical Heat Transfer and Fluid Flow, Washington, DC: Hemisphere Publishing Corp., 1980.

ACKNOWLEDGMENTS

One of us (RES) would like to acknowledge support from the NASA JoVE program.

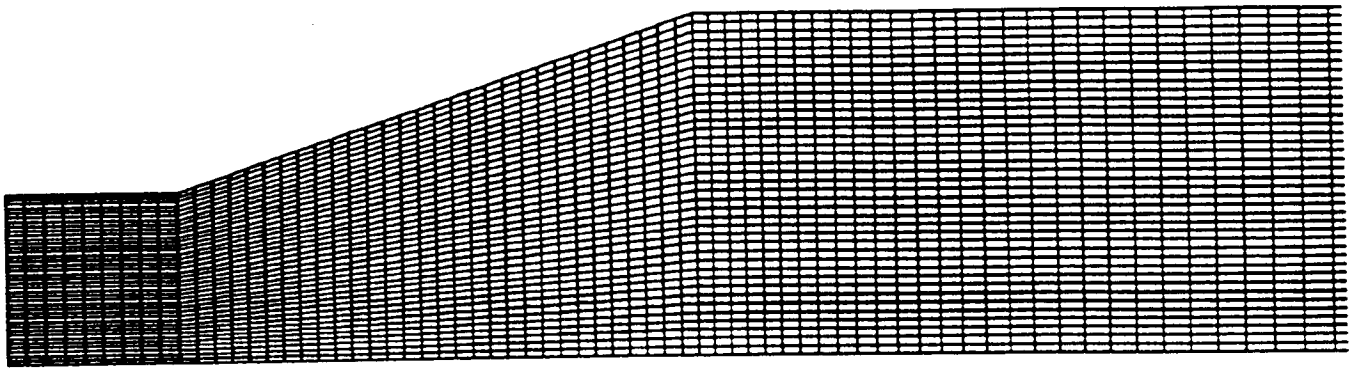

1. Computational grid in the region of vortex breakdown.

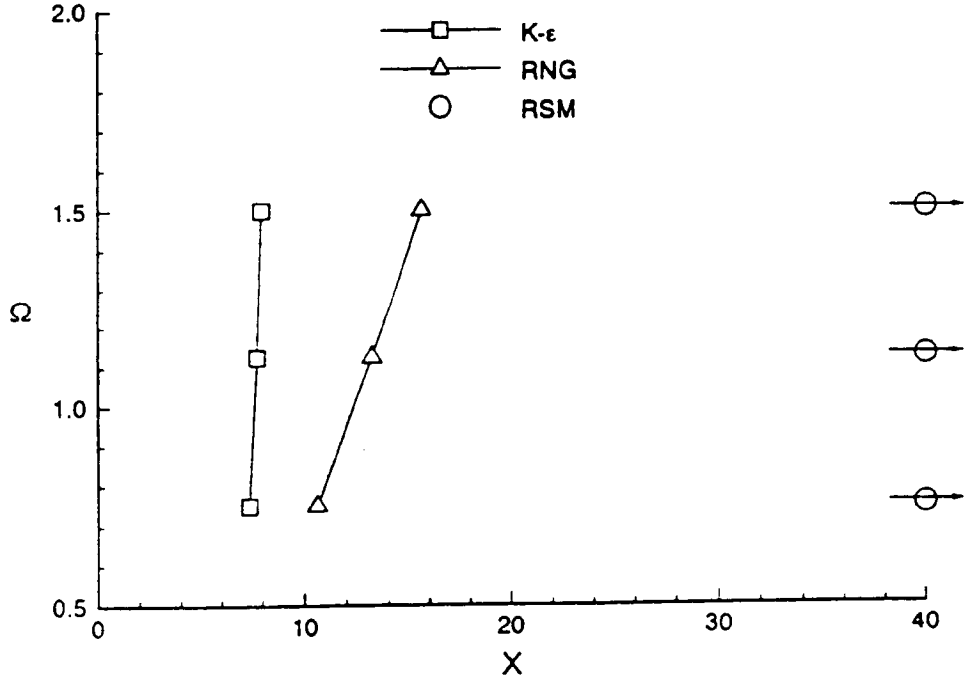

2. Location of return to supercritical conditions as predicted by $K-\varepsilon$, RNG and Reynolds stress turbulence models for strongly swirling flows.

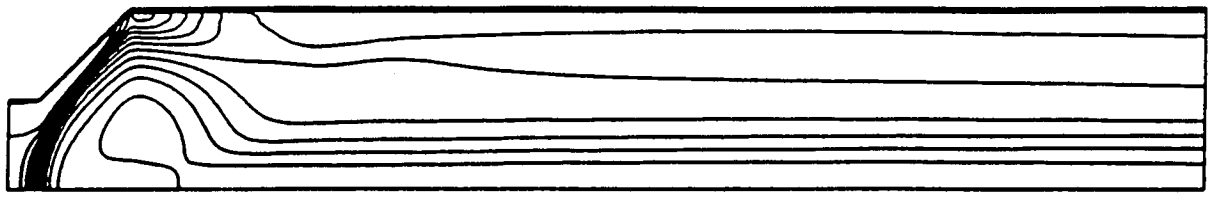

a

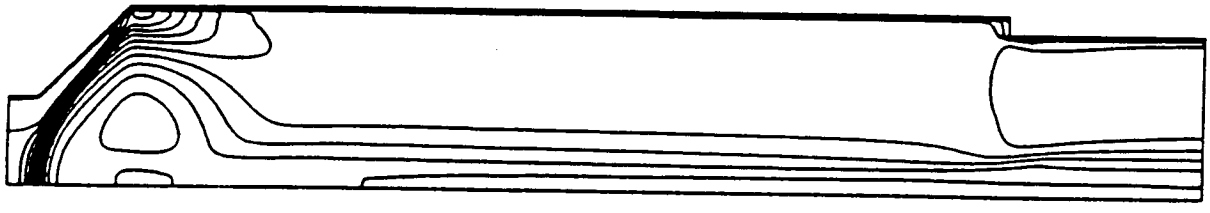

b

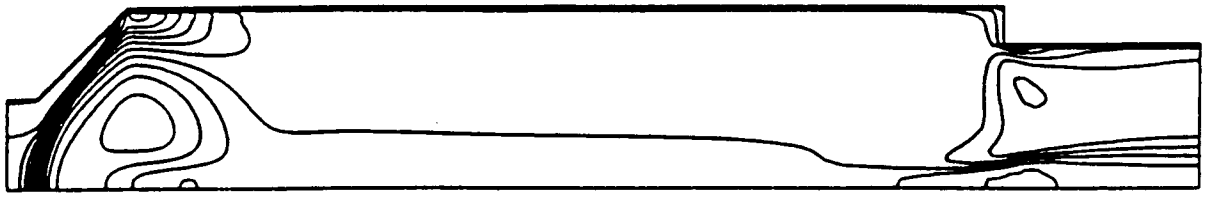

c

3. Contours of constant axial velocity; Reynolds stress model, Ω = 1.5; contour levels from - 0.1 to 1.0 in intervals of 0.1 (geometry scaled by a factor of 3 in the radial direction).
a) No outlet restriction
b) 19% area reduction
c) 36% area reduction

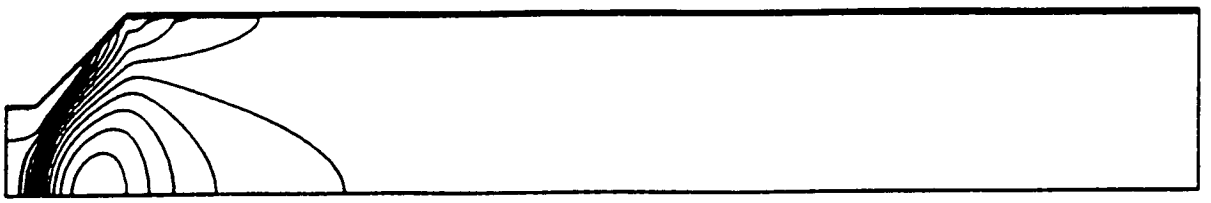

a

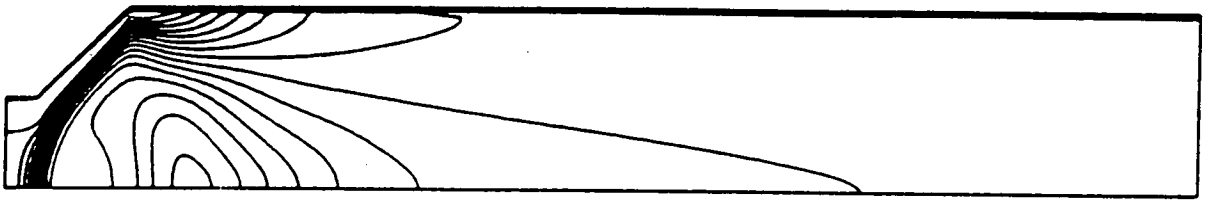

b

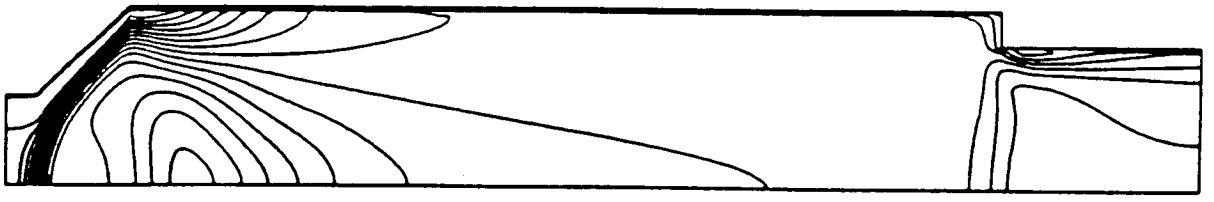

c

4. Contours of constant axial velocity; Ω = 1.5 (geometry scaled by a factor of 3 in the radial direction).
a) $K - \varepsilon$ model; contour levels from -0.2 to 1.0 in intervals of 0.1.
b) RNG model; contour levels from -0.4 to 1.0 in intervals of 0.1.
c) RNG model; 36% area reduction; contour levels from -0.4 to 1.0 in intervals of 0.1.